IEEE Access
Multidisciplinary | Rapid Review | Open Access Journal

Date of publication xxxx 00, 0000, date of current version xxxx 00, 0000.

Digital Object Identifier xxxx/ACCESS.2019.DOI

Alternative Surface Integral Equation-Based Characteristic Mode Formulations for Composite Metallic-Dielectric Objects

SHAODE HUANG[1], JIN PAN[1], YUYUE LUO[1,2], AND DEQIANG YANG[1].
[1]School of Electronic Science and Engineering, University of Electronic Science and Technology of China, Chengdu 611731, China
[2]School of Electrical and Data Engineering, University of Technology Sydney, Australia

This work was supported by the Foundation for Innovative Research Group of the National Natural Science Foundation of China under Grant 61721001. Corresponding author: Jin Pan (e-mail: jpuestc@163.com).

ABSTRACT The characteristic modes (CMs) analysis can give physical insights into the intrinsic mechanisms of radiating structures. To obtain the CMs of composite metallic-dielectric objects is a very challenging task. Existing formulations encounter some problems in calculating the CMs of multiple and multi-layer composite structures. In this paper, we present two new surface integral equation (SIE) formulations for the calculation of CMs of composite metallic-dielectric objects. Employing the contact-region modeling (CRM) technique and the inherent dependent relationships between various kinds of equivalent sources, we propose two new SIE-based CM formulations wherein the electric or magnetic currents on the surfaces of dielectric regions are alternatively involved to suppress spurious modes. Compared to the existing formulations, the proposed formulations are easier to be extended to multiple and multi-layer composite structures. Numerical results of five representative structures are presented to validate the accuracy of the proposed formulations.

INDEX TERMS Surface integral equation (SIE), characteristic modes (CMs), contact-region modeling (CRM), composite metallic-dielectric objects.

I. INTRODUCTION

In recent years, the theory of characteristic modes (TCM) becomes popular in the antenna engineering because it provides a systematic approach to obtain the inherently resonant and modal behaviors of electromagnetic objects, without knowing the definite excitation sources. Thus it can give physical insights into the intrinsic mechanisms of radiating structures. The TCM is initially proposed by Garbacz and Turpin [1], [2] and then reformulated by Harrington and Mautz using the electric field integral equation (EFIE) and the method of moments (MoM) for metallic bodies [3], [4]. We denote the characteristic mode (CM) formulations in [3], [4] as the EFIE-based CM. Following the EFIE-based CM, the TCM was extended to dielectric bodies using the volume integral equation (VIE) [5], named here as the VIE-based CM. However, the VIE-based CM encounters heavy computational burdens when the object's electrical size increased. To speed up the calculation, a surface integral equation (SIE) approach for CMs of dielectric bodies was developed using the Poggio, Miller, Chang, Harrington, Wu, and Tsai (PMCHWT) equation [6], which is denoted as PMCHWT-based CM in this paper. However, the PMCHWT-based CM is found to result in spurious modes [7]. To suppress these spurious modes, two effective methods have been proposed. One is to carry out current elimination according to the dependent relationships between the electric current and magnetic current on the surface of dielectric body [8]–[12]. The other is to select a well-designed weighting matrix that should be expressed as a proper combination of the real and imaginary parts of the radiation related matrix [12]. Note that the formulations in [12] employ both of the two strategies.

Recently, the TCM is extended to the composite metallic-dielectric objects using the SIE approach [13]–[17]. The formulations in [13] are direct combinations of classical TCM formulation for conducting bodies [3] and the TCM formulation for dielectric bodies [12]. The formulations of

This article has been accepted for publication in a future issue of this journal, but has not been fully edited. Content may change prior to final publication. Citation information: DOI 10.1109/ACCESS.2019.2963063, IEEE Access

[13] are only valid for the objects with separated metallic and dielectric parts. The formulations in [14], [15] can be only applied to the fully dielectric-coated objects. The formulations of [16], [17] are applicable to arbitrarily composite metallic-dielectric objects. However, there are two inadequacies of the formulations in [16], [17]:

1) In [16], the current elimination must be carried out to ensure that the final CM formulations only involve a single current. When the object consists of one metal and one dielectric, the electric currents on the surfaces of the metal and the dielectric must be eliminated using the magnetic current on the surface of the dielectric, as shown by (29) and (30) in [16]. If the object is composed of more than one metal and one dielectric, there will be many equivalent currents. It is not clear which current should be the final reserved current in this case. Besides, (29) and (30) in [16] indicate that the current elimination both depends on the media parameters of the dielectric and the geometries of the metal and the dielectric, which means the formulations of current elimination should be reorganized if there are more than one metal and one dielectric. That is, the formulations in [16] failed to be directly applied to the object consists of more than one metal and one dielectric.
2) In [17], by picking a well-designed weighting matrix, the single-current formulation is not necessary. However, the current elimination can not be avoided if the object includes fully dielectric-coated parts. The equivalent sources on the internal interface should be eliminated using the ones on the external interface in this case, as shown by (38) in [17]. If the object is multi-layer structures, to perform the current elimination is complex. The formulation to carry out the current elimination for arbitrarily multi-layer structures was not given in [17] and it was left unanswered. This manipulation of current elimination makes the formulation in [17] difficult to be extended to multi-layer structures.

In this paper, we propose two novel SIE-based formulations for the CMs of composite metallic-dielectric objects. The contact-region modeling (CRM) technique is used to decompose the composite structures as the combination of separated regions [18]. By employing the CRM technique, we found that the current elimination between the equivalent sources on the internal interfaces and the external interfaces can be avoided when the object includes fully dielectric-coated parts. However, the current elimination between the electric and magnetic currents on the same surface of the dielectric body is still required to suppress the spurious modes. Fortunately, with the surface equivalence principle, we found that the current elimination only depends on the geometry of the dielectric, which makes the proposed formulations easier to be extended to multiple and multi-layer composite objects, compared with the approaches in [16], [17]. It is the main advantage of the proposed approach over the methods of [16], [17]. Numerical results of several representative structures are presented to demonstrate the validity and accuracy of the proposed formulations. It is observed that the proposed methods can correctly provide the modal behaviors of composite metallic-dielectric objects, including but not limited to degenerations, resonant frequencies, modal surface currents, modal field distributions, and modal radiation patterns. The proposed methods are expected to be helpful in analyzing and designing the antennas with metallic-dielectric combinations.

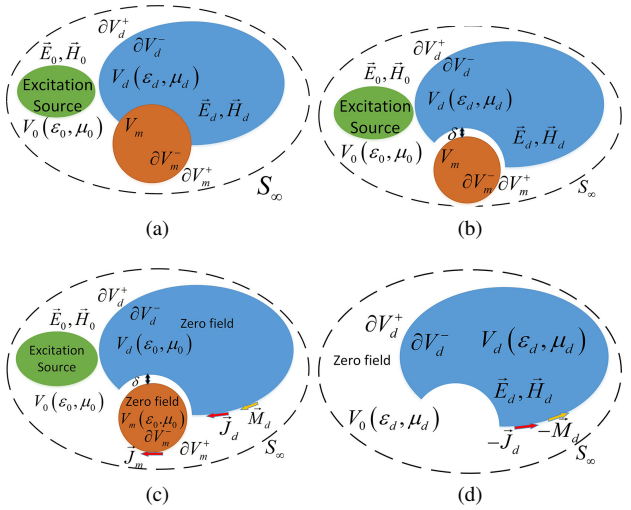

FIGURE 1: Configuration of a composite metallic-dielectric structure and its equivalent situations. (a) Original problem. (b) The equivalent problem with CRM technique. (c) External equivalent situation. (d) Interior equivalent situation.

II. FORMULATIONS

In this section, we propose two new SIE formulations for the CMs of composite metallic-dielectric objects. Before that, the EFIE-PMCHWT formulation with CRM technique (EFIE-PMCHWT-CRM) is briefly reviewed. Next, by applying the surface equivalence principle in each dielectric region, we derive the dependent relationships between the equivalent surface electric and magnetic currents of dielectric bodies. Substituting the dependent relationships into the EFIE-PMCHWT-CRM formulation, we obtain two new SIE formulations, in which the electric or magnetic currents of dielectric bodies are alternatively involved. Finally, based on the two SIE formulations, two new CM formulations are proposed.

A. SIE FORMULATIONS

Without loss of generality, we consider a composite metallic-dielectric structure, as shown in Fig. 1a. The metallic-dielectric object is embedded in a background medium with parameters (ϵ_0, μ_0). The permittivity and permeability of the dielectric body are ϵ_d and μ_d, respectively. Note that the ϵ_d and μ_d could be complex numbers when the material body

This article has been accepted for publication in a future issue of this journal, but has not been fully edited. Content may change prior to final publication. Citation information: DOI 10.1109/ACCESS.2019.2963063, IEEE Access

IEEE Access
Multidisciplinary | Rapid Review | Open Access Journal

is lossy, and the proposed methods still work. The regions occupied by the metallic and dielectric body are V_m and V_d, respectively. Let ∂V_i^+ $\left(\partial V_i^-\right)$ represents the external (interior) surface of the region V_i. We assume the object is excited by a source that exists in the background medium. Let $\left(\vec{E}_{inc}, \vec{H}_{inc}\right)$ denotes the incident field, which is defined as the field that would exist in the absence of the scatter.

With the CRM technique, the original object can be regarded as a simple combination of the separated metallic and dielectric regions, as displayed in Fig. 1b. We use δ to represent the virtual distance between the metallic and dielectric regions. As the value of δ approaches to zero, the problem becomes the same as the original problem [16], [18]. Particularly, $\delta \neq 0$ indicates that the two regions have no contact with each other, and the formulations in this paper still work. Note that the δ is just a virtual distance to illustrate the CRM technique. We don't need to determine the value of δ in the numerical implementation. By decomposing the composite object into separated metallic and dielectric regions, the metallic and dielectric regions can be respectively modeled by using the EFIE and the PMCHWT formulation.

In Fig. 1c, the total fields in the region V_m and V_d are assumed to be zero, and the total fields in the region V_0 remain unchanged. Therefore, the following SIE can be derived

$$\begin{cases} -j\omega\mu_0\mathbf{L}_{dd}^0\left(\vec{J}_d\right) - \mathbf{K}_{dd}^{0+}\left(\vec{M}_d\right) - j\omega\mu_0\mathbf{L}_{dm}^0\left(\vec{J}_m\right) \\ \qquad\qquad + \vec{E}_{inc} = 0,\ on\ \partial V_d^- \\ \mathbf{K}_{dd}^{0+}\left(\vec{J}_d\right) - j\omega\varepsilon_0\mathbf{L}_{dd}^0\left(\vec{M}_d\right) + \mathbf{K}_{dm}^{0-}\left(\vec{J}_m\right) \\ \qquad\qquad + \vec{H}_{inc} = 0,\ on\ \partial V_d^- \\ -j\omega\mu_0\mathbf{L}_{md}^0\left(\vec{J}_d\right) - \mathbf{K}_{md}^{0-}\left(\vec{M}_d\right) - j\omega\mu_0\mathbf{L}_{mm}^0\left(\vec{J}_m\right) \\ \qquad\qquad + \vec{E}_{inc} = 0,\ on\ \partial V_m^- \end{cases} \tag{1}$$

in which

$$\begin{cases} \vec{J}_m = \hat{n}\times\vec{H}_0,\ on\ \partial V_m^+ \\ \vec{J}_d = \hat{n}\times\vec{H}_0,\ on\ \partial V_d^+ \\ \vec{M}_d = \vec{E}_0\times\hat{n},\ on\ \partial V_d^+ \\ \mathbf{L}_{mn}^i\left(\vec{X}\right) = \left(1 + \frac{1}{{k_i}^2}\nabla\nabla\cdot\right)\int_{\partial V_n} G_i\left(\vec{r},\vec{r}'\right)\vec{X}\left(\vec{r}'\right)d\Omega' \\ \mathbf{K}_{mn}^{i\pm}\left(\vec{X}\right) = \pm\frac{\hat{n}}{2}\times\vec{X}\left(\vec{r}\right) \\ \qquad + P.V.\int_{\partial V_n}\nabla G_i\left(\vec{r},\vec{r}'\right)\times\vec{X}\left(\vec{r}'\right)d\Omega' \end{cases} \tag{2}$$

where $\hat{n}$ is the outward unit normal vector, k_i is the wave number in the region V_i, G_i is the Green's function for the homogeneous medium with parameters (ε_i, μ_i), and the subscript $(\cdot)_{mn}$ indicates that the field points and the source points locate on ∂V_m and ∂V_n, respectively. The $P.V.$ represents the Cauchy principal value of the integration. The residue term $\pm\frac{\hat{n}}{2}\times\vec{X}$ should be included in the CRM technique if the field points and the source points locate on the same surface [18]. When the field points approach the source points along the direction of $\hat{n}$, the superscript of $\mathbf{K}$ is plus, otherwise it is minus.

In Fig. 1d, the total fields in the region V_m and V_0 are assumed to be zero, and the total fields in the region V_m remain unchanged. Therefore, we have:

$$\begin{cases} j\omega\mu_d\mathbf{L}_{dd}^d\left(\vec{J}_d\right) + \mathbf{K}_{dd}^{d-}\left(\vec{M}_d\right) = 0,\ on\ \partial V_d^+ \\ -\mathbf{K}_{dd}^{d-}\left(\vec{J}_d\right) + j\omega\varepsilon_d\mathbf{L}_{dd}^d\left(\vec{M}_d\right) = 0,\ on\ \partial V_d^+. \end{cases} \tag{3}$$

Summing (1) and (3), the EFIE-PMCHWT-CRM formulation can be derived:

$$\mathbf{Z}\cdot\begin{bmatrix} J_d \\ M_d \\ J_m \end{bmatrix} = \begin{bmatrix} E_{inc},\ on\ \partial V_d \\ H_{inc},\ on\ \partial V_d \\ E_{inc},\ on\ \partial V_m \end{bmatrix} = g \tag{4}$$

where

$$\mathbf{Z} = \begin{bmatrix} j\omega\mu_0\mathbf{L}_{dd}^0 + j\omega\mu_d\mathbf{L}_{dd}^d & \mathbf{K}_{dd}^{0+} + \mathbf{K}_{dd}^{d-} & j\omega\mu_0\mathbf{L}_{dm}^0 \\ -\mathbf{K}_{dd}^{0+} - \mathbf{K}_{dd}^{d-} & j\omega\varepsilon_0\mathbf{L}_{dd}^0 + j\omega\varepsilon_d\mathbf{L}_{dd}^d & \mathbf{K}_{dm}^{0-} \\ j\omega\mu_0\mathbf{L}_{md}^0 & \mathbf{K}_{md}^{0-} & j\omega\mu_0\mathbf{L}_{mm}^0 \end{bmatrix}. \tag{5}$$

In (4) and (5), it is assumed that we have transformed the operator equation into the matrix equation using the MoM [19], and the same goes for following sections. As a result, $\mathbf{Z}$, $\mathbf{L}$, and $\mathbf{K}$ are matrices. J_d, M_d, J_m, E_{inc}, H_{inc}, and g are column vectors. In this paper, the basis functions and testing functions both are Rao-Wilton-Glisson (RWG) functions [20]. Note that (4) is identical to (6) in [16].

The EFIE-PMCHWT-CRM formulation had been validated for solving scattering problems [18]. However, it cannot be directly used for computing the CMs. The EFIE-PMCHWT-CRM formulation involves three kinds of currents that are not independent, according to (3). More specifically, once the $\vec{J}_d$ is obtained, the $\vec{M}_d$ can be immediately solved using $\vec{J}_d$ without considering incident fields, and vice versa. If the dependent relationships between the $\vec{J}_d$ and $\vec{M}_d$ are not involved when solving the CMs, it would result in some extra modes that violate (3). These extra modes don't exist in the real world and can be recognized as spurious modes. More details about the spurious modes can be found in [11].

According to (3), the dependent relationships between the J_d and M_d can be derived as follows:

$$\begin{cases} J_d = \mathbf{T}\cdot M_d;\ M_d = \mathbf{T}^{-1}\cdot J_d \\ \mathbf{T} = -\left(j\omega\mu_d\mathbf{L}_{dd}^d - \mathbf{K}_{dd}^{d-}\right)^{-1}\cdot\left(j\omega\varepsilon_d\mathbf{L}_{dd}^d + \mathbf{K}_{dd}^{d-}\right). \end{cases} \tag{6}$$

As can be observed from (6), the dependent relationships are irrelevant to the incident fields. Besides, the relationships only depend on the geometry and media parameters of the dielectric itself, and they are uncorrelated with the metal or other dielectric bodies. It is the major difference between our formulations and the ones in [16]. As shown by (30) in [16], the dependent relationships in [16] both depend on the media parameters of the dielectric and the geometries of the metal

This article has been accepted for publication in a future issue of this journal, but has not been fully edited. Content may change prior to final publication. Citation information: DOI 10.1109/ACCESS.2019.2963063, IEEE Access

and the dielectric. It makes the formulations in [16] challenging to be extended to multiple and composite structures. It should be highlighted that the dependent relationships (6) are improved forms of (46) and (49) in [10]. Equations (46) and (49) in [10] are derived by using (44) and (47) in [10]. Equation (6) in this paper can be obtained by summing (44) and (47) of [10]. We found that the dependent relationships (6) of this paper produced more accurate solutions than (46) and (49) in [10]. Equations (44) and (47) in [10] are related to the boundary conditions of electric field and magnetic field, respectively. When summing (44) and (47), the dependent relationships utilize both of the boundary conditions of electric and magnetic field. This is the reason for the better results of the dependent relationships in (6) of this paper.

Substituting (6) into (4), we can derive two novel SIE formulations in which the J_d or the M_d is alternatively involved:

$$\mathbf{Z_J} \cdot \begin{bmatrix} J_d \\ J_m \end{bmatrix} = \begin{bmatrix} \mathbf{I} & \mathbf{0} \\ \mathbf{T}^{-1} & \mathbf{0} \\ \mathbf{0} & \mathbf{I} \end{bmatrix}^H \cdot g = g_J \tag{7}$$

$$\mathbf{Z_M} \cdot \begin{bmatrix} M_d \\ J_m \end{bmatrix} = \begin{bmatrix} \mathbf{T} & \mathbf{0} \\ \mathbf{I} & \mathbf{0} \\ \mathbf{0} & \mathbf{I} \end{bmatrix}^H \cdot g = g_M \tag{8}$$

in which

$$\mathbf{Z_J} = \begin{bmatrix} \mathbf{I} & \mathbf{0} \\ \mathbf{T}^{-1} & \mathbf{0} \\ \mathbf{0} & \mathbf{I} \end{bmatrix}^H \cdot \mathbf{Z} \cdot \begin{bmatrix} \mathbf{I} & \mathbf{0} \\ \mathbf{T}^{-1} & \mathbf{0} \\ \mathbf{0} & \mathbf{I} \end{bmatrix} \tag{9}$$

$$\mathbf{Z_M} = \begin{bmatrix} \mathbf{T} & \mathbf{0} \\ \mathbf{I} & \mathbf{0} \\ \mathbf{0} & \mathbf{I} \end{bmatrix}^H \cdot \mathbf{Z} \cdot \begin{bmatrix} \mathbf{T} & \mathbf{0} \\ \mathbf{I} & \mathbf{0} \\ \mathbf{0} & \mathbf{I} \end{bmatrix} \tag{10}$$

where $\mathbf{I}$ represents the identity matrix, $\mathbf{0}$ represents the zero matrix, and $(\cdot)^H$ represents the conjugate transpose. For convenience, in the following sections, we denote the two SIE formulations in (7) and (8) as SIE-J and SIE-M, respectively.

B. CMS FORMULATIONS

The CMs can be immediately obtained using the following two generalized eigenvalue equations:

$$\mathbf{X_J} \cdot \begin{bmatrix} J_d \\ J_m \end{bmatrix}_n = \lambda_n \mathbf{R_J} \cdot \begin{bmatrix} J_d \\ J_m \end{bmatrix}_n \tag{11}$$

$$\mathbf{X_M} \cdot \begin{bmatrix} M_d \\ J_m \end{bmatrix}_n = \lambda_n \mathbf{R_M} \cdot \begin{bmatrix} M_d \\ J_m \end{bmatrix}_n \tag{12}$$

where $\mathbf{R_i} = \frac{1}{2}\left(\mathbf{Z_i} + \mathbf{Z_i}^H\right)$, $\mathbf{X_i} = \frac{1}{2j}\left(\mathbf{Z_i} - \mathbf{Z_i}^H\right)$, and i= J or M. Equations (11) and (12) result in two kinds of CMs, named here as the SIE-J-based CM and the SIE-M-based CM, respectively. Numerical results in Section III show that both of the two kinds of CMs can provide accurate modal behaviors, which are verified by the commercial software FEKO [21] and other available data. However, the proposed formulations also have limitation. The eigenvectors obtained from the proposed methods may be complex rather than real, because $\mathbf{R_i}$ and $\mathbf{X_i}$ are Hermitian but not symmetric.

Multiplying (7) by $\begin{bmatrix} J_d \\ J_m \end{bmatrix}^H$, we have

$$\begin{aligned} &\begin{bmatrix} J_d \\ J_m \end{bmatrix}^H \cdot \mathbf{Z_J} \cdot \begin{bmatrix} J_d \\ J_m \end{bmatrix} \\ &= \begin{bmatrix} J_d \\ J_m \end{bmatrix}^H \cdot \begin{bmatrix} \mathbf{I} & \mathbf{0} \\ \mathbf{T}^{-1} & \mathbf{0} \\ \mathbf{0} & \mathbf{I} \end{bmatrix}^H \cdot g \\ &= \begin{bmatrix} J_d \\ M_d \\ J_m \end{bmatrix}^H \cdot g \end{aligned} \tag{13}$$

Substituting g of (4) into (13) results in

$$\begin{aligned} &\begin{bmatrix} J_d \\ J_m \end{bmatrix}^H \cdot \mathbf{Z_J} \cdot \begin{bmatrix} J_d \\ J_m \end{bmatrix} \\ &= \begin{bmatrix} J_d \\ M_d \\ J_m \end{bmatrix}^H \cdot \begin{bmatrix} E_{inc},\ on\ \partial V_d \\ H_{inc},\ on\ \partial V_d \\ E_{inc},\ on\ \partial V_m \end{bmatrix} \\ &= \left\langle \vec{J}_d^*, \vec{E}_{inc} \right\rangle_{\partial V_d} + \left\langle \vec{M}_d^*, \vec{H}_{inc} \right\rangle_{\partial V_d} + \left\langle \vec{J}_m^*, \vec{E}_{inc} \right\rangle_{\partial V_m} \end{aligned} \tag{14}$$

Based on (5) and (36) in [10], it is found that

$$\begin{aligned} &\frac{1}{2}\left[\left\langle \vec{J}_d^*, \vec{E}_{inc} \right\rangle_{\partial V_d} + \left\langle \vec{M}_d^*, \vec{H}_{inc} \right\rangle_{\partial V_d} + \left\langle \vec{J}_m^*, \vec{E}_{inc} \right\rangle_{\partial V_m}\right] \\ &= P_{rad} + jP_{reac} \end{aligned} \tag{15}$$

in which P_{rad} and P_{reac} represent the radiated power and reactive power, respectively. Finally, we have

$$\frac{1}{2}\begin{bmatrix} J_d \\ J_m \end{bmatrix}^H \cdot \mathbf{Z_J} \cdot \begin{bmatrix} J_d \\ J_m \end{bmatrix} = P_{rad} + jP_{reac} \tag{16}$$

According to the definition of $\mathbf{R_J}$ and $\mathbf{X_J}$, it is obvious that

$$\frac{1}{2}\begin{bmatrix} J_d \\ J_m \end{bmatrix}^H \cdot \mathbf{R_J} \cdot \begin{bmatrix} J_d \\ J_m \end{bmatrix} = P_{rad} \tag{17}$$

$$\frac{1}{2}\begin{bmatrix} J_d \\ J_m \end{bmatrix}^H \cdot \mathbf{X_J} \cdot \begin{bmatrix} J_d \\ J_m \end{bmatrix} = P_{reac} \tag{18}$$

Multiplying (11) by $\begin{bmatrix} J_d \\ J_m \end{bmatrix}_n^H$, it can be found that

$$\lambda_n = \frac{\begin{bmatrix} J_d \\ J_m \end{bmatrix}_n^H \cdot \mathbf{X_J} \cdot \begin{bmatrix} J_d \\ J_m \end{bmatrix}_n}{\begin{bmatrix} J_d \\ J_m \end{bmatrix}_n^H \cdot \mathbf{R_J} \cdot \begin{bmatrix} J_d \\ J_m \end{bmatrix}_n} = \frac{P_{reac}}{P_{rad}} \tag{19}$$

This article has been accepted for publication in a future issue of this journal, but has not been fully edited. Content may change prior to final publication. Citation information: DOI 10.1109/ACCESS.2019.2963063, IEEE Access

IEEE Access
Multidisciplinary | Rapid Review | Open Access Journal

Equation (19) proves that the eigenvalues of the SIE-J-based CM represent the ratios between the reactive power and the radiated power of corresponding modes. Similar properties can be also found for the SIE-M-based CM.

Once we have computed the CMs, any surface currents can be written as the linear combinations of the CMs. Let us take the SIE-J-based CM as an example. Because that both $\mathbf{R_J}$ and $\mathbf{X_J}$ are Hermitian matrices, the eigenvectors are orthogonal according to the Corollary 4.6.12 of [22]:

$$\begin{cases} \begin{bmatrix} J_d \\ J_m \end{bmatrix}_m^H \cdot \mathbf{R_J} \cdot \begin{bmatrix} J_d \\ J_m \end{bmatrix}_n = \delta_{mn} \\ \begin{bmatrix} J_d \\ J_m \end{bmatrix}_m^H \cdot \mathbf{X_J} \cdot \begin{bmatrix} J_d \\ J_m \end{bmatrix}_n = \lambda_n \delta_{mn} \\ \begin{bmatrix} J_d \\ J_m \end{bmatrix}_m^H \cdot \mathbf{Z_J} \cdot \begin{bmatrix} J_d \\ J_m \end{bmatrix}_n = (1 + j\lambda_n)\, \delta_{mn} \end{cases} \tag{20}$$

where δ_{mn} is the Kronecker delta (0 if $m \neq n$, and 1 if $m = n$). For simplify, it is assumed that the eigenvectors are normalized according to: $\begin{bmatrix} J_d \\ J_m \end{bmatrix}_n^H \cdot \mathbf{R_J} \cdot \begin{bmatrix} J_d \\ J_m \end{bmatrix}_n = 1$. Equation (20) demonstrates that both of the radiated powers and reactive powers of the obtained CMs are orthogonal.

Substituting the orthogonality into (7), we can derive the expansion coefficients of the CMs:

$$\begin{bmatrix} J_d \\ J_m \end{bmatrix} = \sum_n \alpha_n \begin{bmatrix} J_d \\ J_m \end{bmatrix}_n \tag{21}$$

in which

$$\begin{aligned} \alpha_n &= \frac{1}{1+j\lambda_n} \begin{bmatrix} J_d \\ J_m \end{bmatrix}_n^H \cdot g_J \\ &= \frac{\left\langle \left[\vec{J}_d\right]_n^*, \vec{E}_{inc} \right\rangle + \left\langle \left[\vec{M}_d\right]_n^*, \vec{H}_{inc} \right\rangle + \left\langle \left[\vec{J}_m\right]_n^*, \vec{E}_{inc} \right\rangle}{1+j\lambda_n} \end{aligned} \tag{22}$$

The surface magnetic current M_d can be obtained using (6). As can be observed from (22), the expansion coefficients are composed of two parts. The numerator is related to the coupling between the modal currents and the incident fields. The denominator is only relevant to the eigenvalue, thus it is the inherent property of CMs. Besides, the denominator of (22) indicates that those λ_n with smaller magnitudes are more important for the radiation and scattering problems, especially those resonant modes with $\lambda_n = 0$. To investigate the resonant behavior over a wide frequency band, the modal significance (MS, defined as $\left|\frac{1}{1+j\lambda}\right|$) is more convenient than λ_n. The modes with MS approach to 1 are resonant.

C. MULTIPLE AND COMPOSITE STRUCTURES

Compared to the existing SIE-based CM formulations for metallic-dielectric objects, the proposed formulations provide a natural and straightforward way to handle multiple and multi-layer composite structures because we employ the CRM technique and the intrinsic dependent relationships between the electric and magnetic currents on the surfaces of dielectric bodies. As an example, consider a composite structure with one metal and two homogeneous dielectric regions. The media parameters of the two dielectric regions are (ε_1, μ_1) and (ε_2, μ_2), respectively. The surfaces of the two dielectric regions and metal region are ∂V_{d1}, ∂V_{d2}, and ∂V_{m1}. The EFIE-PMCHWT-CRM equation in this case becomes:

$$\mathbf{Z} \cdot \begin{bmatrix} J_{d1} \\ M_{d1} \\ J_{d2} \\ M_{d2} \\ J_{m1} \end{bmatrix} = \begin{bmatrix} E_{inc},\ on\ \partial V_{d1} \\ H_{inc},\ on\ \partial V_{d1} \\ E_{inc},\ on\ \partial V_{d2} \\ H_{inc},\ on\ \partial V_{d2} \\ E_{inc},\ on\ \partial V_{m1} \end{bmatrix} = g \tag{23}$$

where

$$\mathbf{Z} = \begin{bmatrix} \mathbf{Z_{d1d1}} & \mathbf{Z_{d1d2}} & \mathbf{Z_{d1m1}} \\ \mathbf{Z_{d2d1}} & \mathbf{Z_{d2d2}} & \mathbf{Z_{d2m1}} \\ \mathbf{Z_{m1d1}} & \mathbf{Z_{m1d2}} & \mathbf{Z_{m1m1}} \end{bmatrix} \tag{24}$$

in which

$$\begin{cases} \mathbf{Z_{d1d1}} = \begin{bmatrix} j\omega\mu_0 \mathbf{L}^0_{d1d1} + j\omega\mu_1 \mathbf{L}^{d1}_{d1d1} & \mathbf{K}^{0+}_{d1d1} + \mathbf{K}^{d1-}_{d1d1} \\ -\mathbf{K}^{0+}_{d1d1} + \mathbf{K}^{d1-}_{d1d1} & j\omega\varepsilon_0 \mathbf{L}^0_{d1d1} - j\omega\varepsilon_1 \mathbf{L}^{d1}_{d1d1} \end{bmatrix} \\ \mathbf{Z_{d1d2}} = \begin{bmatrix} j\omega\mu_0 \mathbf{L}^0_{d1d2} & \mathbf{K}^{0-}_{d1d2} \\ -\mathbf{K}^{0-}_{d1d2} & j\omega\varepsilon_0 \mathbf{L}^0_{d1d2} \end{bmatrix} \\ \mathbf{Z_{d1m1}} = \begin{bmatrix} j\omega\mu_0 \mathbf{L}^0_{d1m1} \\ -\mathbf{K}^{0-}_{d1m1} \end{bmatrix} \\ \mathbf{Z_{d2d1}} = \begin{bmatrix} j\omega\mu_0 \mathbf{L}^0_{d2d1} & \mathbf{K}^{0-}_{d2d1} \\ -\mathbf{K}^{0-}_{d2d1} & j\omega\varepsilon_0 \mathbf{L}^0_{d2d1} \end{bmatrix} \\ \mathbf{Z_{d2d2}} = \begin{bmatrix} j\omega\mu_0 \mathbf{L}^0_{d2d2} + j\omega\mu_2 \mathbf{L}^{d2}_{d2d2} & \mathbf{K}^{0+}_{d2d2} + \mathbf{K}^{d2-}_{d2d2} \\ -\mathbf{K}^{0+}_{d2d2} + \mathbf{K}^{d2-}_{d2d2} & j\omega\varepsilon_0 \mathbf{L}^0_{d2d2} - j\omega\varepsilon_2 \mathbf{L}^{d2}_{d2d2} \end{bmatrix} \\ \mathbf{Z_{d2m1}} = \begin{bmatrix} j\omega\mu_0 \mathbf{L}^0_{d2m1} \\ -\mathbf{K}^{0-}_{d2m1} \end{bmatrix} \\ \mathbf{Z_{m1d1}} = \begin{bmatrix} j\omega\mu_0 \mathbf{L}^0_{m1d1} & \mathbf{K}^{0-}_{m1d1} \end{bmatrix} \\ \mathbf{Z_{m1d2}} = \begin{bmatrix} j\omega\mu_0 \mathbf{L}^0_{m1d2} & \mathbf{K}^{0-}_{m1d2} \end{bmatrix} \\ \mathbf{Z_{m1m1}} = j\omega\mu_0 \mathbf{L}^0_{m1m1} \end{cases} \tag{25}$$

Employing the surface equivalence principle, the inherent dependent relationships between J_{di} and M_{di} $(i = 1, 2)$ are:

$$\begin{cases} J_{di} = \mathbf{T_i} \cdot M_{di};\ M_{di} = \mathbf{T_i}^{-1} \cdot J_{di} \\ \mathbf{T_i} = -\left(j\omega\mu_i \mathbf{L}^{di}_{didi} - \mathbf{K}^{di-}_{didi}\right) \cdot \left(j\omega\varepsilon_i \mathbf{L}^{di}_{didi} + \mathbf{K}^{di-}_{didi}\right) \end{cases} \tag{26}$$

Obviously, the dependent relationships between J_{di} and M_{di} only depended on the media parameters and geometry of the dielectric region i. Substituting (26) into (23), the SIE-J and SIE-M equation can be obtained:

$$\mathbf{Z_J} \cdot \begin{bmatrix} J_{d1} \\ J_{d2} \\ J_{m1} \end{bmatrix} = \begin{bmatrix} \mathbf{I} & \mathbf{0} & \mathbf{0} \\ \mathbf{T_1}^{-1} & \mathbf{0} & \mathbf{0} \\ \mathbf{0} & \mathbf{I} & \mathbf{0} \\ \mathbf{0} & \mathbf{T_2}^{-1} & \mathbf{0} \\ \mathbf{0} & \mathbf{0} & \mathbf{I} \end{bmatrix}^H \cdot g = g_J \tag{27}$$

This article has been accepted for publication in a future issue of this journal, but has not been fully edited. Content may change prior to final publication. Citation information: DOI 10.1109/ACCESS.2019.2963063, IEEE Access

$$\mathbf{Z_M} \cdot \begin{bmatrix} M_{d1} \\ M_{d2} \\ J_{m1} \end{bmatrix} = \begin{bmatrix} \mathbf{T_1} & \mathbf{0} & \mathbf{0} \\ \mathbf{I} & \mathbf{0} & \mathbf{0} \\ \mathbf{0} & \mathbf{T_2} & \mathbf{0} \\ \mathbf{0} & \mathbf{I} & \mathbf{0} \\ \mathbf{0} & \mathbf{0} & \mathbf{I} \end{bmatrix}^H \cdot g = g_M \tag{28}$$

in which

$$\mathbf{Z_J} = \begin{bmatrix} \mathbf{I} & \mathbf{0} & \mathbf{0} \\ \mathbf{T_1^{-1}} & \mathbf{0} & \mathbf{0} \\ \mathbf{0} & \mathbf{I} & \mathbf{0} \\ \mathbf{0} & \mathbf{T_2^{-1}} & \mathbf{0} \\ \mathbf{0} & \mathbf{0} & \mathbf{I} \end{bmatrix}^H \cdot \mathbf{Z} \cdot \begin{bmatrix} \mathbf{I} & \mathbf{0} & \mathbf{0} \\ \mathbf{T_1^{-1}} & \mathbf{0} & \mathbf{0} \\ \mathbf{0} & \mathbf{I} & \mathbf{0} \\ \mathbf{0} & \mathbf{T_2^{-1}} & \mathbf{0} \\ \mathbf{0} & \mathbf{0} & \mathbf{I} \end{bmatrix} \tag{29}$$

$$\mathbf{Z_M} = \begin{bmatrix} \mathbf{T_1} & \mathbf{0} & \mathbf{0} \\ \mathbf{I} & \mathbf{0} & \mathbf{0} \\ \mathbf{0} & \mathbf{T_2} & \mathbf{0} \\ \mathbf{0} & \mathbf{I} & \mathbf{0} \\ \mathbf{0} & \mathbf{0} & \mathbf{I} \end{bmatrix}^H \cdot \mathbf{Z} \cdot \begin{bmatrix} \mathbf{T_1} & \mathbf{0} & \mathbf{0} \\ \mathbf{I} & \mathbf{0} & \mathbf{0} \\ \mathbf{0} & \mathbf{T_2} & \mathbf{0} \\ \mathbf{0} & \mathbf{I} & \mathbf{0} \\ \mathbf{0} & \mathbf{0} & \mathbf{I} \end{bmatrix} \tag{30}$$

Finally, the SIE-J-based CM and the SIE-M-based CM are obtained using (11) and (12).

III. NUMERICAL RESULTS

To demonstrate the validity and accuracy of the proposed formulations, the modal behaviors of five composite structures with metallic-dielectric combinations are investigated using the FEKO and the proposed formulations. To ensure that the results of FEKO are immune from spurious modes, we set the equivalent sources of dielectric regions as volumetric currents in FEKO. The results of FEKO are taken as the reference solution, because of its well-known ability to give the reliable modal solutions, despite its heavy computational burden [15]. The five objects represent five different types of electromagnetic structures:

1) Fully dielectric-coated metal
2) Fully dielectric-coated dielectric bodies
3) Dielectric bodies partially coated with metal
4) Multiple metals with one dielectric body
5) Multiple dielectric bodies with one metal

A. FULLY DIELECTRIC-COATED METAL

We first compute the CMs of a hemispherical dielectric resonator antenna (DRA) with a concentric conductor, as displayed in Fig. 2. The fundamental mode of the hemispherical DRA is the TE_{111} mode, whose modal behaviors have been investigated using either analytic method [23] or TCM [14]–[16]. Benefiting from the image theory and the symmetry of the TE_{111} mode, we can remove the ground plane and regard the DRA as a fully dielectric-coated conducting sphere without changing the modal behaviors of the TE_{111} mode [14]–[16].

Fig. 3 shows the MS curves of the first 50 modes obtained from the FEKO, the proposed formulations, and the formulations in [16], [17]. There are many degenerate modes owing to the symmetry of the antenna. In Fig. 3, we label the resonant frequencies and degeneracy (inside the parenthesis), and mark the higher-order modes by black circles. The

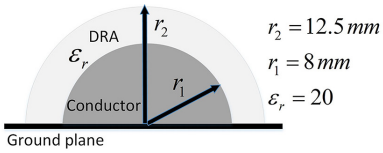

FIGURE 2: Sectional view of a hemispherical DRA with a concentric conductor.

resonant frequencies are identified by locating the maximal values of the MS. The numerical solution of an analytical expression reveals that the resonant frequency of TE_{111} mode is 4.218 GHz [23]. From Fig. 3, we observed that the resonant frequency of the TE_{111} mode obtained from the FEKO, the proposed formulations, and the formulation in [17] are 4.25 GHz, which coincide with the resonant frequency reported in [23]. Furthermore, the MS curves of the proposed formulations are similar to those of FEKO and the formulation in [17], which validates the proposed formulations in this case. However, the MS curves obtained from the formulations of [16] are not similar with those of the proposed formulations. It is because that the formulations of [16] sometimes result in spurious modes, as reported in [15]. Note that the MS of the higher-order modes is slightly different between the FEKO and the proposed methods. It is caused by the relatively coarse mesh used in FEKO. The VIE is used to model the dielectric regions in FEKO to ensure that the results are reliable [15]. We have to choose a relatively coarse mesh in FEKO to decrease the unknowns because that a fine mesh of the VIE requires huge memories which exceeds the maximum memory of our computer. In the numerical calculations of this paper, the average tetrahedron edge length in FEKO equals $\frac{\lambda}{8}$, and the average triangle edge length in the proposed method is $\frac{\lambda}{10}$, where λ is the wavelength in the dielectric region at the highest frequency. If the average tetrahedron edge length in FEKO is $\frac{\lambda}{10}$, there might be more than 60000 unknowns for the first example, which is unbearable for our computer. Fortunately, the slight difference of MS curves doesn't affect the resonant frequencies, as can be observed from the MS curves.

Besides, we plot the surface currents, the three-dimensional radiation patterns, and the cut-plane radiation patterns of the resonant modes at 4.25 GHz obtained from the FEKO and the proposed methods in Fig. 4 to 6. In Fig. 4 and 5, the colors indicate the relative intensities of various quantities. The red denotes the maximum values, and the blue represents the minimum values. We use normalized scale in the figures for comparison. The maximum values are normalized to 1. It can be observed that the three modes at 4.25 GHz obtained from the proposed formulations are degenerate modes. Good agreement is found between the results of the proposed methods and the FEKO. In addition, the radiation patterns are similar to those of dipole antennas, and are consistent with the radiation pattern of TE_{111} mode of the spherical DRA.

This article has been accepted for publication in a future issue of this journal, but has not been fully edited. Content may change prior to final publication. Citation information: DOI 10.1109/ACCESS.2019.2963063, IEEE Access

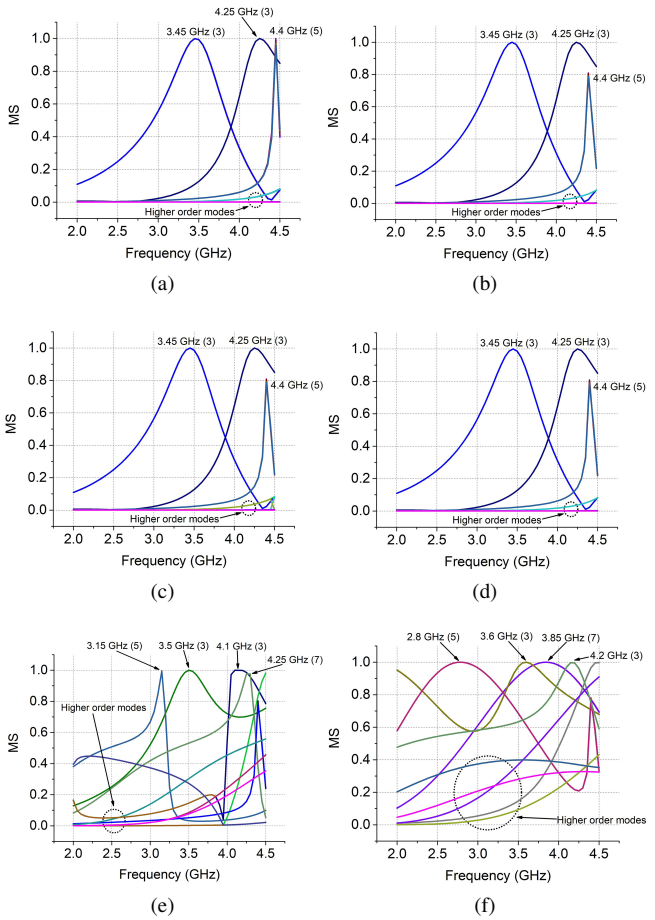

FIGURE 3: The MS of the first 50 modes of the hemispherical DRA obtained from different methods. (a) FEKO. (b) SIE-J-based CM obtained from (11). (c) SIE-M-based CM obtained from (12). (d) Equation (39) of [17]. (e) Equation (45) of [16]. (f) Equation (34) of [16].

Differently from the FEKO, the proposed SIE-based CM formulations only define unknowns on the surfaces of objects. Therefore they can abate the computational burdens. In this example, there are 32772 unknowns in the FEKO, while only 4464 unknowns in the proposed formulations. The computing time of the FEKO and the proposed methods are 413 seconds and 21 seconds, respectively. The computing time includes the time for the computation of the impedance matrix and solving the generalized eigenvalue equation at a single frequency.

B. FULLY DIELECTRIC-COATED DIELECTRIC SPHERE

As the second test, we consider a two-layer spherical DRA as an example of fully dielectric-coated dielectric objects. Its configuration is shown in Fig. 7. The MS of the first 50 modes obtained from the FEKO and the proposed methods are depicted in Fig. 8. It is clear that the FEKO and the proposed methods provide the similar MS curves. The MS curves indicate that the resonant frequency of the dominant

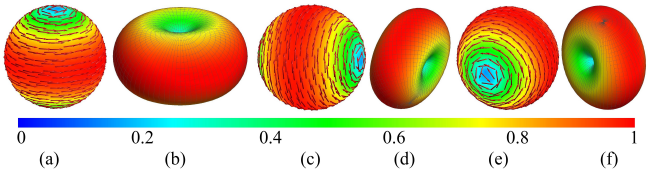

FIGURE 4: Modal behaviors obtained from the FEKO at 4.25 GHz. (a) Mode 1's electric current on the surface of conductor. (b) Mode 1's radiation pattern. (c) Mode 2's electric current on the surface of conductor. (d) Mode 2's radiation pattern. (e) Mode 3's electric current on the surface of conductor. (f) Mode 3's radiation pattern.

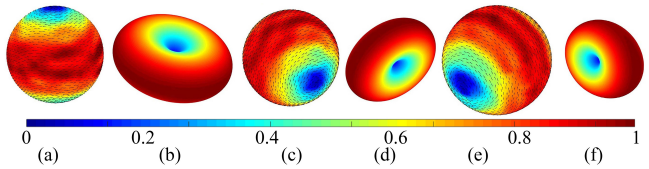

FIGURE 5: Modal behaviors obtained from the proposed methods at 4.25 GHz. (a) Mode 1's electric current on the surface of dielectric coating. (b) Mode 1's radiation pattern. (c) Mode 2's electric current on the surface of dielectric coating. (d) Mode 2's radiation pattern. (e) Mode 3's electric current on the surface of dielectric coating. (f) Mode 3's radiation pattern.

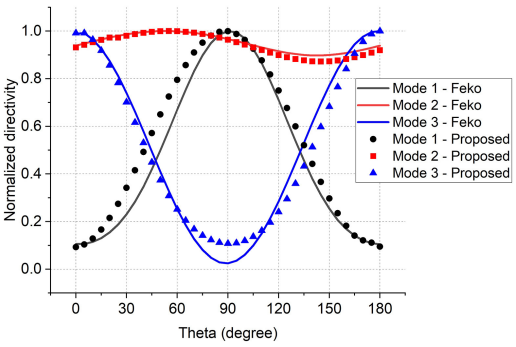

FIGURE 6: The cut-plane ($\phi = 0$) radiation patterns of the resonant modes at 4.25 GHz obtained from the proposed methods and the FEKO.

mode is 1.8 GHz, which agrees with the resonant frequency of TE_{111} mode reported in [24]. Besides, the MS curves shown in Fig. 8 reveal that there are several degenerate modes at the lowest resonant frequency. We plot the electric fields inside the dielectric regions, magnetic fields inside the dielectric regions, and radiation patterns of all three modes obtained from the FEKO and the proposed approaches at the lowest resonant frequency 1.8 GHz in Fig. 9 and 10. It can be observed that the distributions of the fields and the radiation patterns of the proposed methods are consistent with those obtained from the FEKO. Furthermore, the modal behaviors displayed in Fig. 10 coincide with those of TE_{111} mode. The accordance again verifies that the proposed methods can

This article has been accepted for publication in a future issue of this journal, but has not been fully edited. Content may change prior to final publication. Citation information: DOI 10.1109/ACCESS.2019.2963063, IEEE Access

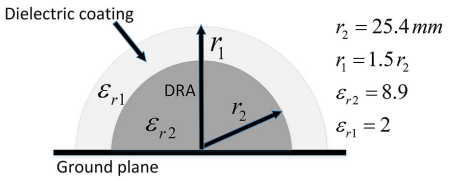

FIGURE 7: Configuration of a two-layer spherical DRA.

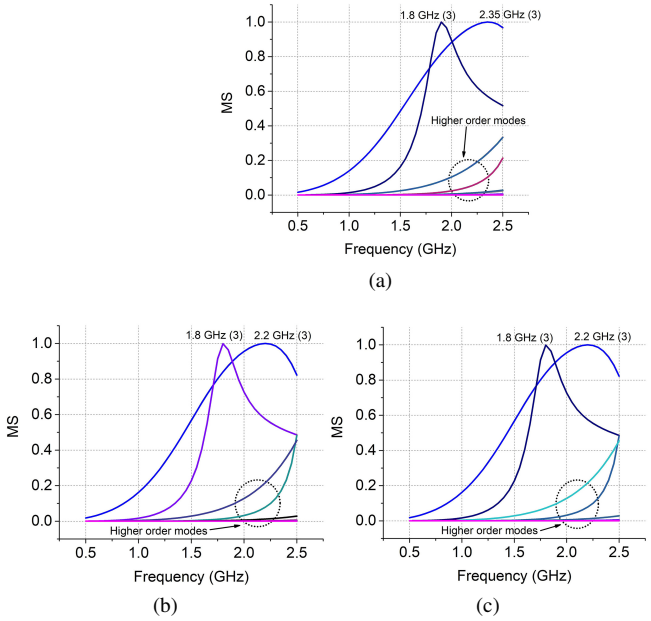

FIGURE 8: The MS of the first 50 modes of the two-layer spherical DRA obtained from different methods. (a) FEKO. (b) SIE-J-based CM obtained from (11). (c) SIE-M-based CM obtained from (12).

provide accurate modal behaviors of the two-layer DRA.

C. DIELECTRIC CUBOID PARTIALLY COATED WITH METALLIC SHEETS

In this example, we consider a cuboid DRA partially coated with two metallic sheets, as shown in Fig. 11. The parameters are $W = 25.4\ mm$, $h = 6.35\ mm$, and $\epsilon_r = 9.2$. Fig. 12 shows The MS of the first 50 modes obtained from the FEKO and the proposed methods. It is found that the MS curves of the proposed methods agree well with those of the FEKO. The MS curves shown in Fig. 12 indicate that the resonant frequency of the dominant mode is 2.05 GHz, which is in accordance with the measured resonant frequency 2.08 GHz reported in [25], [26]. In addition, it can be observed in Fig. 12 that there are degenerate modes at 2.05 GHz. We plot the electric currents on the metallic plates and radiation patterns of the dominant modes obtained from the FEKO and the proposed methods in Fig. 13 to 14, which verifies that the modal behaviors obtained from the FEKO and the proposed approaches are identical.

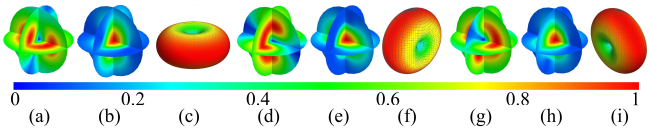

FIGURE 9: Modal behaviors obtained from the FEKO at 1.8 GHz. (a) Electric field of Mode 1. (b) Magnetic field of Mode 1. (c) Radiation pattern of Mode 1. (d) Electric field of Mode 2. (e) Magnetic field of Mode 2. (f) Radiation pattern of Mode 2. (g) Electric field of Mode 3. (h) Magnetic field of Mode 3. (i) Radiation pattern of Mode 3.

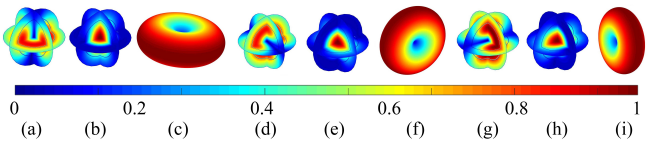

FIGURE 10: Modal behaviors obtained from the proposed methods at 1.8 GHz. (a) Electric field of Mode 1. (b) Magnetic field of Mode 1. (c) Radiation pattern of Mode 1. (d) Electric field of Mode 2. (e) Magnetic field of Mode 2. (f) Radiation pattern of Mode 2. (g) Electric field of Mode 3. (h) Magnetic field of Mode 3. (i) Radiation pattern of Mode 3.

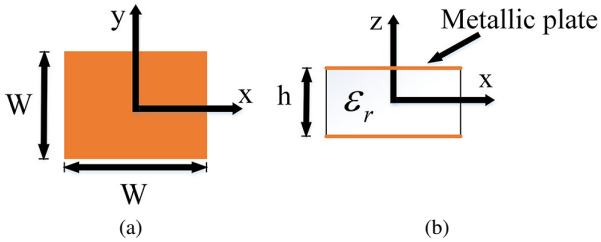

FIGURE 11: Geometry of the dielectric cuboid partially coated with metallic sheet. (a) Top view. (b) Side view.

D. MULTIPLE METALS WITH ONE DIELECTRIC BODY

To demonstrate the generality of our formulations, we investigate the modal behaviors of a ring DRA loaded with a metallic rod in its center and two metallic caps on its top and bottom surfaces, as shown in Fig. 15. The top and the cross-sectional view of the DRA are displayed in Fig. 1a in [27]. The parameters of the antenna configurations refer to Section II and Table I in [27]. The inner radius $R_i = 2$ mm is selected, i.e., cap 4 in [27]. The feed probe of the antenna studied in [27] is the metallic rod of the antenna simulated in this case. We herein assume that the ground plane is infinite thus we can remove the ground plane based on the image theory.

The MS of the first 50 modes obtained from the FEKO and the proposed methods are depicted in Fig. 16. It can be found that the MS obtained from the FEKO and the proposed approaches are identical. The MS curves indicate that the resonant frequency of the DRA is 5.35 GHz, which agrees with the simulated and measured results in [27]. In addition,

This article has been accepted for publication in a future issue of this journal, but has not been fully edited. Content may change prior to final publication. Citation information: DOI 10.1109/ACCESS.2019.2963063, IEEE Access

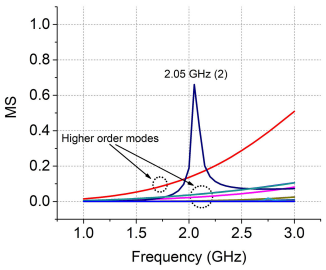

(a)

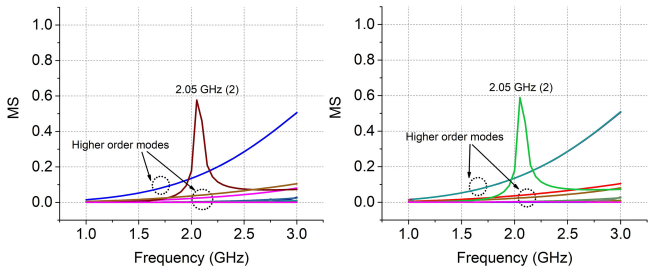

(b) (c)

FIGURE 12: The MS of the first 50 modes of the cuboid DRA obtained from different methods. (a) FEKO. (b) SIE-J-based CM obtained from (11). (c) SIE-M-based CM obtained from (12).

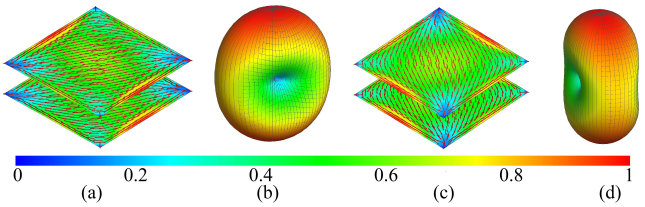

(a) (b) (c) (d)

FIGURE 13: Modal behaviors obtained from the FEKO at 2.05 GHz. (a) Electric currents on the metallic plates of Mode 1. (b) Radiation pattern of Mode 1. (c) Electric currents on the metallic plates of Mode 2. (d) Radiation pattern of Mode 2.

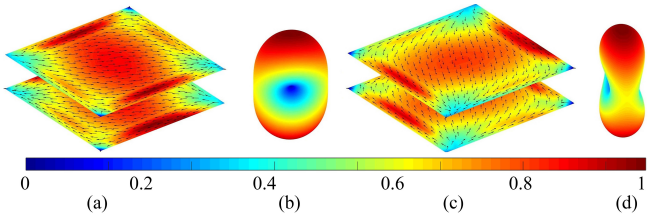

(a) (b) (c) (d)

FIGURE 14: Modal behaviors obtained from the proposed methods at 2.05 GHz. (a) Electric currents on the metallic plates of Mode 1. (b) Radiation pattern of Mode 1. (c) Electric currents on the metallic plates of Mode 2. (d) Radiation pattern of Mode 2.

we plot the electric currents on the metallic parts and the radiation pattern of the resonant mode obtained from the FEKO and the proposed approaches in Fig. 17. It can be observed that the modal currents and patterns obtained from

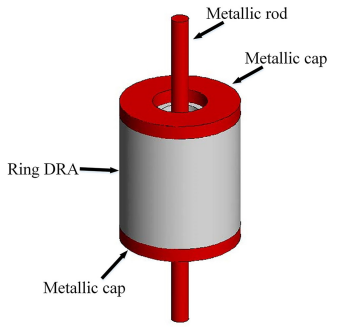

FIGURE 15: The isotropic view of a ring DRA loaded with a metallic rod in its center and two metallic caps on its top and bottom surfaces.

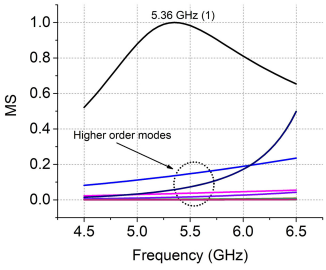

(a)

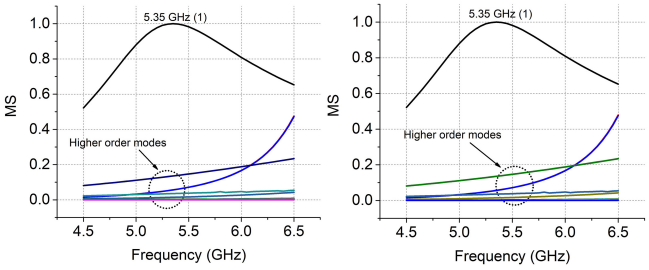

(b) (c)

FIGURE 16: The MS of the first 50 modes of the ring DRA loaded with multi PEC obtained from different methods. (a) FEKO. (b) SIE-J-based CM obtained from (11). (c) SIE-M-based CM obtained from (12).

the FEKO and the proposed methods are almost identical. Furthermore, the modal currents and patterns presented in Fig. 17 coincide with the simulated and measured results reported in [27]. The results prove that we use the image theory to remove the ground plane is valid.

E. MULTIPLE DIELECTRIC BODIES WITH ONE METAL

As the final example, we consider a three-layer structure as an example of the multiple dielectric bodies with one metal. The object is composed of a concentric spherical conductor with two-layer dielectric coatings. The relative permittivities of the coatings are 20 and 10, respectively. Its sectional view is illustrated in Fig. 18. We depict the MS of the first 50 modes obtained from the FEKO and the proposed methods

This article has been accepted for publication in a future issue of this journal, but has not been fully edited. Content may change prior to final publication. Citation information: DOI 10.1109/ACCESS.2019.2963063, IEEE Access

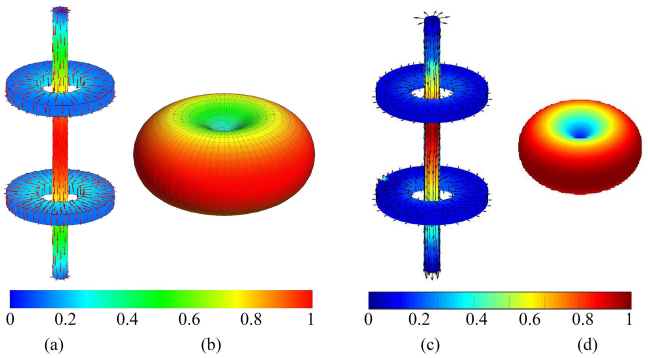

FIGURE 17: Current and radiation pattern of the resonant mode obtained from the FEKO and the proposed methods. (a) Electric current on the metallic parts obtained from the FEKO. (b) Radiation pattern obtained from the FEKO. (c) Electric current on the metallic parts obtained from the proposed methods. (d) Radiation pattern obtained from the proposed methods.

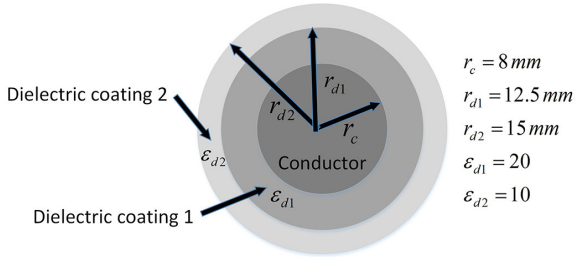

FIGURE 18: Sectional view of a concentric conductor with two-layer dielectric coatings.

in Fig. 19. It is observed that they result in the similar MS curves, which reveal that the lowest resonant frequency is 2.85 GHz. We plot the electric currents (on the surface of conductor) and radiation patterns of the three resonant modes obtained from the FEKO and the proposed approaches at the lowest resonant frequency 2.85 GHz in Fig. 20 and 21. As can be observed, the currents and the radiation patterns of the proposed methods are consistent with those obtained from the FEKO.

In summary, the numerical tests of the five representative structures validate that the proposed formulations can provide accurate modal behaviors of composite objects with arbitrarily metallic-dielectric combinations.

IV. CONCLUSION

With the surface equivalence principle and the CRM technique, we propose two new SIE formulations for the calculation of CMs of composite metallic-dielectric objects. The electric or magnetic currents on the surfaces of the dielectric regions are alternatively involved to avoid spurious modes in the proposed formulations. The new formulations are easy to be extended to multi-layer structures. Numerical results prove that the proposed formulations can suppress spurious modes and accurately provide the modal behaviors

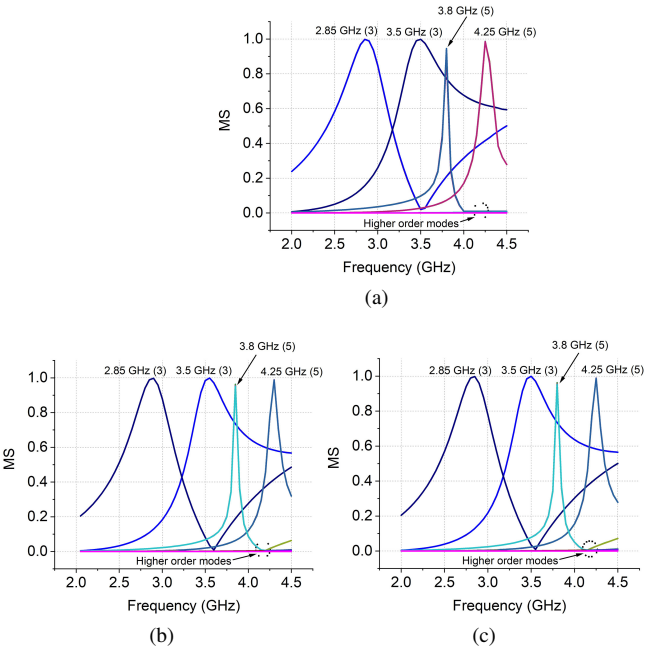

FIGURE 19: The MS of the first 50 modes of the three-layer object obtained from different methods. (a) FEKO. (b) SIE-J-based CM obtained from (11). (c) SIE-M-based CM obtained from (12).

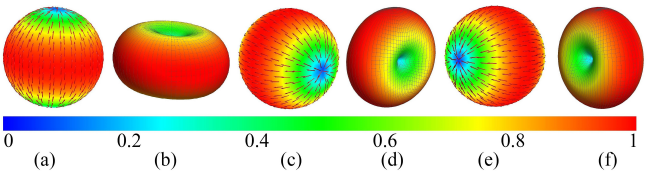

FIGURE 20: Modal behaviors obtained from the FEKO at 2.85 GHz. (a) Mode 1's electric current on the surface of conductor. (b) Mode 1's radiation pattern. (c) Mode 2's electric current on the surface of conductor. (d) Mode 2's radiation pattern. (e) Mode 3's electric current on the surface of conductor. (f) Mode 3's radiation pattern.

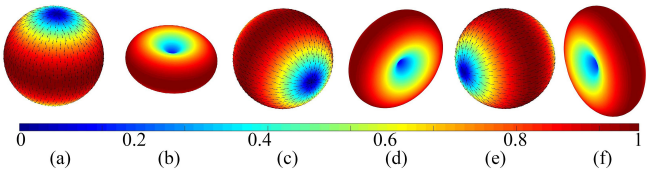

FIGURE 21: Modal behaviors obtained from the proposed methods at 2.85 GHz. (a) Mode 1's electric current on the surface of conductor. (b) Mode 1's radiation pattern. (c) Mode 2's electric current on the surface of conductor. (d) Mode 2's radiation pattern. (e) Mode 3's electric current on the surface of conductor. (f) Mode 3's radiation pattern.

of composite objects. We expect that the proposed CMs formulations would contribute to the analysis and design of practical antennas with metallic-dielectric combinations.

REFERENCES

[1] R. J. Garbacz, "Modal expansions for resonance scattering phenomena," Proceedings of the IEEE, vol. 53, no. 8, pp. 856–864, Aug. 1965.

[2] R. Garbacz and R. Turpin, "A generalized expansion for radiated and scattered fields," IEEE Transactions on Antennas and Propagation, vol. 19, no. 3, pp. 348–358, May 1971.

[3] R. Harrington and J. Mautz, "Theory of characteristic modes for conducting bodies," IEEE Transactions on Antennas and Propagation, vol. 19, no. 5, pp. 622–628, Sep. 1971.

[4] R. Harrington and J. Mautz, "Computation of characteristic modes for conducting bodies," IEEE Transactions on Antennas and Propagation, vol. 19, no. 5, pp. 629–639, Sep. 1971.

[5] R. Harrington, J. Mautz, and Y. Chang, "Characteristic modes for dielectric and magnetic bodies," IEEE Transactions on Antennas and Propagation, vol. 20, no. 2, pp. 194–198, Mar. 1972.

[6] Y. Chang and R. Harrington, "A surface formulation for characteristic modes of material bodies," IEEE Transactions on Antennas and Propagation, vol. 25, no. 6, pp. 789–795, Nov. 1977.

[7] H. Alroughani, J. L. T. Ethier, and D. A. McNamara, "Observations on computational outcomes for the characteristic modes of dielectric objects," in 2014 IEEE Antennas and Propagation Society International Symposium (APSURSI), July 2014, pp. 844–845.

[8] Y. Chen, "Alternative surface integral equation-based characteristic mode analysis of dielectric resonator antennas," IET Microwaves, Antennas Propagation, vol. 10, no. 2, pp. 193–201, 2016.

[9] F. G. Hu and C. F. Wang, "Integral equation formulations for characteristic modes of dielectric and magnetic bodies," IEEE Transactions on Antennas and Propagation, vol. 64, no. 11, pp. 4770–4776, Nov. 2016.

[10] R. Lian, J. Pan, and S. Huang, "Alternative surface integral equation formulations for characteristic modes of dielectric and magnetic bodies," IEEE Transactions on Antennas and Propagation, vol. 65, no. 9, pp. 4706–4716, Sep. 2017.

[11] S. Huang, J. Pan, and Y. Luo, "Investigations of non-physical characteristic modes of material bodies," IEEE Access, vol. 6, pp. 17 198–17 204, 2018.

[12] P. Ylä-Oijala, H. Wallén, D. C. Tzarouchis, and A. Sihvola, "Surface integral equation-based characteristic mode formulation for penetrable bodies," IEEE Transactions on Antennas and Propagation, vol. 66, no. 7, pp. 3532–3539, July 2018.

[13] P. Ylä-Oijala, A. Lehtovuori, H. Wallén, and V. Viikari, "Coupling of characteristic modes on pec and lossy dielectric structures," IEEE Transactions on Antennas and Propagation, vol. 67, no. 4, pp. 2565–2573, April 2019.

[14] L. Guo, Y. Chen, and S. Yang, "Characteristic mode formulation for dielectric coated conducting bodies," IEEE Transactions on Antennas and Propagation, vol. 65, no. 3, pp. 1248–1258, Mar. 2017.

[15] S. Huang, J. Pan, Y. Luo, and D. Yang, "Single-source surface integral equation formulations for characteristic modes of fully dielectric-coated objects," IEEE Transactions on Antennas and Propagation, vol. 67, no. 7, pp. 4914–4919, July 2019.

[16] L. Guo, Y. Chen, and S. Yang, "Generalized characteristic-mode formulation for composite structures with arbitrarily metallic–dielectric combinations," IEEE Transactions on Antennas and Propagation, vol. 66, no. 7, pp. 3556–3566, July 2018.

[17] P. Ylä-Oijala, "Generalized theory of characteristic modes," IEEE Transactions on Antennas and Propagation, vol. 67, no. 6, pp. 3915–3923, June 2019.

[18] Y. Chu, W. C. Chew, J. Zhao, and S. Chen, "A surface integral equation formulation for low-frequency scattering from a composite object," IEEE Transactions on Antennas and Propagation, vol. 51, no. 10, pp. 2837–2844, Oct. 2003.

[19] R. F. Harrington, Field computation by moment methods. Wiley-IEEE Press, 1993.

[20] S. Rao, D. Wilton, and A. Glisson, "Electromagnetic scattering by surfaces of arbitrary shape," IEEE Transactions on Antennas and Propagation, vol. 30, no. 3, pp. 409–418, May 1982.

[21] FEKO. [Online]. Available: https://altairhyperworks.com/product/FEKO

[22] R. A. Horn, R. A. Horn, and C. R. Johnson, Matrix analysis. Cambridge university press, 1990.

[23] K. W. Leung, "Complex resonance and radiation of hemispherical dielectric-resonator antenna with a concentric conductor," IEEE Transactions on Microwave Theory and Techniques, vol. 49, no. 3, pp. 524–531, Mar. 2001.

[24] K.-L. Wong and N.-C. Chen, "Analysis of a broadband hemispherical dielectric resonator antenna with a dielectric coating," Microwave and Optical Technology Letters, vol. 7, no. 2, pp. 73–76, 1994.

[25] A. Petosa, Dielectric resonator antenna handbook. Artech House Publishers, 2007.

[26] R. Mongia, "Reduced size metallized dielectric resonator antennas," in Antennas and Propagation Society International Symposium, 1997. IEEE., 1997 Digest, vol. 4. IEEE, 1997, pp. 2202–2205.

[27] L. A. Shaik, C. Saha, S. Arora, S. Das, J. Y. Siddiqui, and A. K. Iyer, "Bandwidth control of cylindrical ring dielectric resonator antennas using metallic cap and sleeve loading," IET Microwaves, Antennas Propagation, vol. 11, no. 12, pp. 1742–1747, 2017.

SHAODE HUANG was born in Sichuan Province, China, in 1992. He received the B.S. degree in electromagnetic field and microwave technique from the University of Electronic Science and Technology of China (UESTC), Chengdu, China, in 2014, and he is currently working toward the Ph.D. degree. His current research interests include antennas theory and computational electromagnetics.

JIN PAN received the B.S. degree in Electronics and Communication Engineering of Radio Engineering Department, Sichuan University, Chengdu, China, in 1983, then M.S. and Ph.D. degrees in electromagnetic field and microwave technique from UESTC in 1983 and 1986, respectively. From 2000 to 2001, he was a visiting scholar in the Electronics and Communication Engineering of Radio Engineering Department, City University of Hong Kong. He is currently a Full Professor in the School of Electronic Engineering, UESTC. His current research interests include electromagnetic theory and computation, antenna theory and technique, field and wave in inhomogeneous media, microwave remote sensing theory and its applications.

YUYUE LUO was born in Sichuan Province, China, in 1991. She received the B.S degree in electromagnetic field and microwave technique from the University of Electronic Science and Technology of China (UESTC), Chengdu, China, in 2013, and she is currently a Ph.D. candidate of UESTC. Her current research interests include antenna theory and array signal processing.

DEQIANG YANG received the B.S. degree, the M.S. degree and Ph.D. degree in electromagnetic field and microwave technique from the University of Electronic Science and Technology of China (UESTC) in 1992 ,2006 and 2012, respectively. His current research interests include antenna theory and technique, antenna measurement and development of sensors for UWB system.